energy&fuels

pubs.acs.org/EF Article

Using Copper Ore and Hematite Fine Particles as Raw Materials of an Oxygen Carrier for Chemical Looping Combustion of Coal: Spray Drying Granulation and Performance Evaluation

Zhao Su, Yanan Wang, Han Du, Jinchen Ma, Ying Zheng, and Haibo Zhao*

Cite This: *Energy Fuels* 2020, 34, 8587−8599 Read Online

ACCESS | Metrics & More | Article Recommendations

ABSTRACT: Spray drying has gradually become an effective method for large-scale preparation of oxygen carriers as a result of its unique advantages (high efficiency, scalable production, etc.). However, expensive chemical or commercial powder is usually used as raw material in spray drying granulation. The main objective of this work is to reduce the cost of a spray-drying-derived oxygen carrier through using cheap natural ores as raw materials and optimizing the preparation process. Considering that hematite is cheap but less active in chemical looping combustion (CLC) processes, while copper ore has high oxygen carrying capacity and good reactivity but suffers from sintering at a high temperature, the bi-ore oxygen carrier is prepared by the spray drying granulation method in this work using copper ore and hematite fine powders as raw materials with the addition of a suitable dispersant and binder. Two kinds of oxygen carriers are successfully prepared by the spray drying method, Fe100 (the mass ratio of hematite is 100%) and Cu20Fe80 (the mass ratio of copper ore/hematite is 20:80%), and their performance is evaluated in a batch fluidized bed reactor. The reactivity of Cu20Fe80 is superior than that of Fe100 to char gasification products. The effects of the temperature, oxygen/fuel ratio, and coal rank on the coal-derived CLC performance of Cu20Fe80 are further examined. The temperature of 950 °C is the optimal choice with the highest reaction rate and CO_2 yield. The gasification rate is fast using the low-rank coals as fuels, i.e., Chifeng lignite and Shenhua bituminous coal. Moreover, Cu20Fe80 exhibits good stability during the redox test of more than 10 cycles. The used oxygen carrier particles still maintain the abundant pore structure well without the sintering phenomenon. Additionally, the results of scanning electron microscopy with energy-dispersive spectrometry indicate that there is almost no decrease in the relative content of Cu elements after the cyclic tests. This work demonstrates that the spray-drying-derived Cu20Fe80 particle is a promising choice as an oxygen carrier for industrial application of the CLC process.

1. INTRODUCTION

Fossil fuels will remain the main energy source in China,[1] and the reduction of CO_2 emission will be a bottleneck problem for the use of fossil energy. Chemical looping combustion (CLC) uses oxygen carrier (OC) particles to circulate active oxygen and heat between the air reactor and fuel reactor to achieve the cascade utilization of fuel chemical energy[2] and the internal CO_2 separation, which is considered to be an innovative combustion method and CO_2 capture technology in fossil fuel combustion.[3]

In the air reactor, the OCs are oxidized, converting gaseous oxygen into lattice oxygen. Then, active lattice oxygen and heat will be transferred for the oxidation of the hydrocarbon fuel (usually endothermic reaction) in the fuel reactor. Obviously, the high performance (sufficient oxygen-donating capacity, reactivity, durability, etc.) of the OCs are the cornerstone of CLC.[4] Moreover, the demand of OCs is enormous (usually ≥1000 kg/MW_{th}),[5,6] and the lifetime is limited (as a result of attrition, agglomeration, and ash slag removal) in the CLC of coal. Therefore, the OCs in CLC of coal are required to be cheap and abundant. At present, some natural ores have been evaluated in the continuously operated CLC unit, e.g., ilmenite,[6−8] hematite,[9−11] manganese ore,[12−14] etc. However, the direct use of natural ores has some problems, such as low reactivity, easy attrition, and low combustion efficiency. On the other side, synthetic OCs[15,16] demonstrate the better performance than the natural ores. In this case, the high cost of the materials is, however, a limit for the industrial application. In addition, the preparation methods of the OCs include the freezing granulation method,[17,18] mechanical mixing method,[19,20] and impregnation method[21,22] in lab scale at present. It was reported in our previous work that the higher yield was achieved by the freezing granulation method but the preparation period was longer; the impregnation method showed quite a high yield and the shortest preparation period.[23] It is difficult to scale up these preparation methods to an industrial scale.

The spray drying granulation method is a relatively mature industrial method for the production of the catalysts and adsorbents, and the uniformly distributed particles with good sphericity are prepared by this method, which can be used for

Received: March 31, 2020
Revised: June 10, 2020
Published: June 10, 2020

https://dx.doi.org/10.1021/acs.energyfuels.0c01023
Energy Fuels 2020, 34, 8587−8599

the preparation of OCs.[24] The selection of raw materials, including active ingredients and inert carrier, is the key to the preparation of the OC by spray drying. Many kinds of OCs have been synthesized by spray drying, such as Fe-based,[25−27] Ni-based,[28−30] Cu-based,[31,32] and Mn-based[33−35] OCs. The effect of an inert carrier on the performance of OCs has been investigated. Baek et al.[30] compared the physicochemical properties of Ni-based OCs to α-Al_2O_3 or γ-Al_2O_3 as inert materials, separately. The low calcination temperature was optimized, so that the higher specific surface area was achieved when unstable γ-Al_2O_3 was used as the inert material. De Vos et al.[26] found that the inactivation of the OCs was successfully avoided after replacing the inert material from Al_2O_3 to $MgAl_2O_4$ for Fe-based OC. Mattisson et al.[36] found that the oxygen-releasing performance of manganese-ore-based OC was enhanced by adding $Ca(OH)_2$ as an inert carrier. The preparation of the slurry is also important for the spray drying method. De Vos et al.[37] investigated the effect of the preparation process of the slurry on the OC preparation by spray drying. Finally, a satisfactory OC preparation process was obtained by optimizing the solid, binder, and dispersant content. Jing et al.[38] found that the milling time of the slurry showed a non-negligible effect on the crushing strength and bulk density of as-received OCs. Recently, to apply the spray-drying-derived OC for industrial-scale chemical looping, Jacobs et al.[35] developed the industrial-scale spray drying method. The results showed that the prepared manganese-based OCs had a long life and good reactivity. However, most of studies involved in the spray-drying-derived OCs use expensive chemical or commercial powder as raw materials (except that Mattisson et al.[36] used manganese ore as raw materials). Therefore, it is still required to reduce the cost of OC through using the cheap natural ores as raw materials and optimizing the preparation process.

Natural ores (such as iron ore, copper ore, etc.) have been considered as the raw materials of OCs as a result of their desirable characteristics of low cost, sufficient reactivity, and superior fluidization.[39−41] Iron ore, which is very cheap and environmentally friendly, meanwhile demonstrating acceptable reactivity, has been widely tested in the CLC.[6−11] Copper ore, which has high oxygen carrying capacity and good reactivity but is easily sintered and agglomerated, has also been investigated by the CLC community.[42,43] In our previous work, Yang et al.[20] physically mixed copper ore and hematite particles as the OC, which showed higher reactivity and desirable synergy compared to hematite or copper ore as the OC alone. In addition, the proper mixing proportion of copper ore and hematite had the characteristic of thermal neutrality when the mass ratio of copper ore/hematite was 2:8. Within the multiple redox cycles, not only was the sintering resistance of CuO enhanced but the reduction degree of Fe_2O_3 was also increased.[44] To avoid the segregation of the physically mixed bi-ore powders and achieve the synergistic effect within a single particle, Tian et al.[45] used copper ore and hematite fine particles as the raw material, cement as both the binder and inert material to prepare the OC; the synergistic effect was still held when the hematite/copper ore ratio was 80:20 wt %; the fluidized bed tests also showed that the cement-bonded bi-ore OC had better reactivity and satisfying durability. However, the cement bonding method requires quite a long time to harden the bulk products, which deserves further improvement when used for large-scale OC preparation.

Thus, this work focuses on the batch preparation of the OCs by the spray drying granulation method, using the copper ore and hematite fine particles as the materials (less than 100 μm). Generally, the particle size of suitable OCs in the fluidized bed should be controlled to about 150−350 μm to achieve a good fluidization performance. However, some crushed ore particles or industrial waste powders cannot be directly used because of the small particle size, irregular shape, etc. Therefore, using fine powders of copper ore and hematite as the main raw materials of the OC in this work represents a kind of waste reutilization indeed. Once the OC is successfully prepared through spray drying granulation, the reactivity and stability of as-received OCs are tested in a batch fluidized bed reactor. The OCs are characterized by X-ray diffraction (XRD), environmental scanning electron microscopy (ESEM), scanning electron microscopy with energy-dispersive spectrometry (SEM−EDS), and Brunauer−Emmett−Teller (BET) analysis before and after the reaction.

2. EXPERIMENTAL SECTION

2.1. Materials. The copper ore and hematite fine powders with the size below 100 μm are combined by the spray drying granulation method to produce OCs in a suitable size range. To improve the mechanical strength and remove sulfur contained in refined copper ore, the raw materials are calcined at 500 °C for 5 h and then at 1000 °C for 10 h with the heating rate of 5 °C/min in an air atmosphere.[46] The chemical compositions of the copper ore and hematite are presented in Table 1, examined by X-ray fluorescence (XRF, FP-6500, Japan). Polyvinylalcohol (PVA) is selected as the binder to combine the fine particles to form large particles with a satisfying target size during spray drying. Ammonium citrate is used as the dispersant to improve the rheology of the slurry.

Table 1. Chemical Compositions of the Copper Ore and Hematite

hematite (wt %)		copper ore (wt %)	
Fe_2O_3	90.65	CuO	34.09
SiO_2	4.73	Fe_2O_3	59.36
Al_2O_3	1.16	SiO_2	3.08
others	3.46	Al_2O_3	1.02
		others	2.45

Three kinds of coal are tested, i.e., Chifeng (CF) lignite, Shenhua (SH) bituminous coal, and Shanxi (SX) anthracite. The coal is dried at 105 °C for 10 h in a vacuum drying oven and then sieved to the particle size of 0.2−0.3 mm. The proximate and ultimate analyses of the coal are shown in Table 2.

2.2. Preparation Process. According to our previous studies,[20,45] the mass ratio of copper ore/hematite is also selected as 2:8 here, and the prepared composite OC is denoted as Cu20Fe80. The similar process is also used to prepare the OC with only hematite as the raw material, denoted as Fe100. The theoretical maximum oxygen transport capacities of Fe100 and Cu20Fe80 are calculated to be 3.02 and 3.49%, respectively.

The specific process of spray drying granulation is described as follows: (1) Preparation of slurry: Copper ore and hematite (d_p < 100 μm) are dispersed in water with a dispersant (dispersant can be saved if the suspension properties of materials are good). To obtain a smaller size of raw materials and uniform solution, the suspensions are ball-milled in a planetary ball mill with stainless milling balls. Afterward, binder (PVA here) is added to enhance the viscosity of the slurry to prepare large particles during spray drying. (2) Spray drying process: The prepared slurry is continuously stirred as it is pumped into the bottom of the drying chamber through a two-fluid spray nozzle and then mixes with the heated air to form particles. The air is

https://dx.doi.org/10.1021/acs.energyfuels.0c01023
Energy Fuels 2020, 34, 8587−8599

Table 2. Proximate and Ultimate Analyses of Coals

	proximate analysis (wt %, ad)				ultimate analysis (wt %, ad)			
coal	moisture	volatile matter	fixed carbon	ash	C	H	S	N
CF	2.67	42.61	38.43	16.29	54.58	3.91	1.79	0.93
SH	2.22	38.33	41.08	18.36	51.22	2.01	0.41	0.24
SX	1.01	12.31	51.07	35.61	56.15	3.28	2.34	1.08

preheated in the range of 200−220 °C to prevent the formation of hollow particles at too high of a temperature during the spray drying process. (3) Screening and calcination: The particles in the range of 150−350 μm are screened for the calcination process. Finally, the spray-drying-derived granules are calcined at 500 °C for 5 h and then at 1100 °C for 10 h with the heating rate of 5 °C/min in an air atmosphere to increase the mechanical strength. The main parameters of steps 1 and 2 are shown in Table 3.

Table 3. Operating Parameters of Spray Drying

air inlet temperature (°C)	gas pressure in the nozzle (MPa)	solid content (vol %[a])	binder (wt %[b])	dispersant (wt %[b])
200−220	0.1	37.5−45.5	1.2−1.8	0.8−1.4

[a]In comparison to the total volume of the suspension. [b]In comparison to the total amount of solid.

2.3. Experiments in a Fluidized Bed Reactor. The reaction tests are performed in a batch fluidized bed reactor, which consists of the main reactor, gas supply system, and exhaust gas analysis system. Figure 1 presents a schematic of the batch fluidized bed. The main reaction zone is 835 mm in height and 28 mm for inner diameter. The air distribution plate is placed above 470 mm of the bottom. The gas supply system is composed of three kinds of gases (air, N_2, and H_2O) to simulate the CLC process. A mixture of 50 vol % nitrogen and 50 vol % steam is used as the gasification and fluidization agent in the reduction stage; air is used as the oxidization gas in the oxidation process; and nitrogen is used to purge the reactor after each redox cycle. The gas flow rate in all periods is controlled at 2 L/min by a mass flow meter, which corresponds to about 4−9 times the minimum fluidization velocity of the particles. The fine particles and steam in the exhaust gas from the reactor are removed by the water solution and electrical condenser, respectively. The online gas analyzer (Gasboard Analyzer 3100, Cubic) is used to determine the concentrations of CO_2, CO, CH_4, O_2, and H_2, within the range of 0−10 vol % for CO, CH_4, and H_2, 0−25 vol % for O_2, and 0−100 vol % for CO_2. The measurement accuracy is 1% of full scale, and the gas information collection interval is 1 s.

The experimental conditions are shown in Table 4. The temperature window is set as 850−950 °C. The oxygen/fuel ratio (ϕ) is in the range of 1.5−2.5. Three kinds of coal with various ranks are used as the solid fuel, and the Fe100 and Cu20Fe80 particles are used as OCs. With respect to the experimental procedure, a certain amount of OC particles is placed on the air distribution plate first and then heated to the setting value in the air atmosphere (2 L/min) for 30 min to ensure that the OCs are completely oxidized by the air. Subsequently, the fluidization gas is switched to a mixture of 50 vol %

Table 4. Experimental Conditions

case number	OC type	coal type	ϕ	mass of coal (g)	temperature (°C)
1	Fe100	SH	2.5	0.36	950
2	Cu20Fe80	SH	1.5	0.59	950
3	Cu20Fe80	SH	2.0	0.44	950
4	Cu20Fe80	SH	2.5	0.36	950
5	Cu20Fe80	SH	2.5	0.36	900
6	Cu20Fe80	SH	2.5	0.36	850
7	Cu20Fe80	CF	2.0	0.46	950
8	Cu20Fe80	SX	2.0	0.40	950

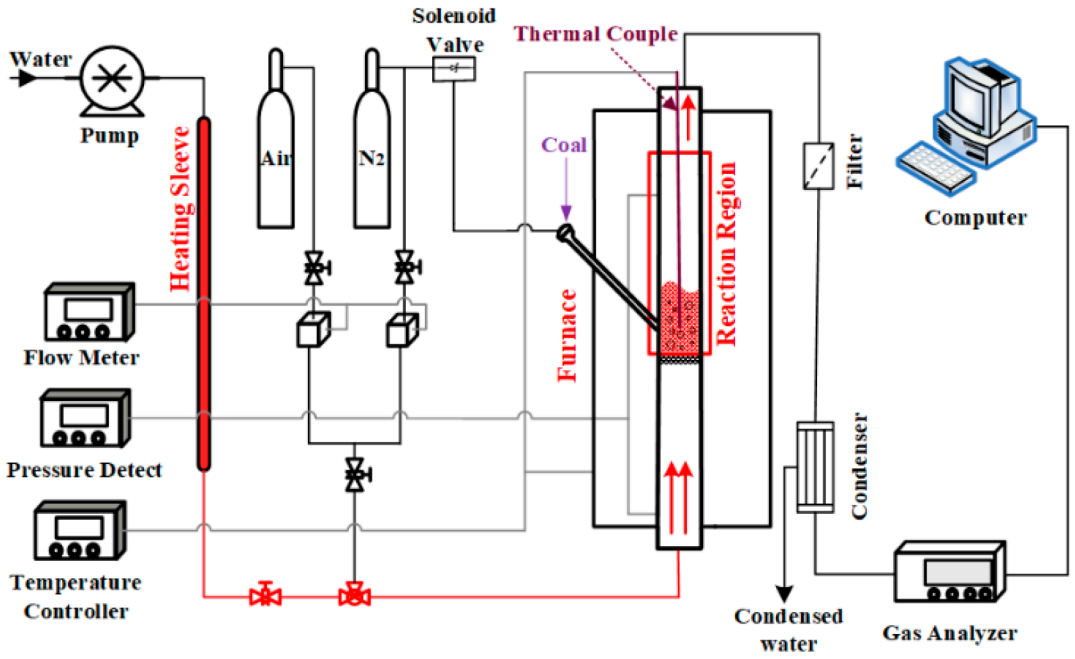

Figure 1. Schematic layout of the batch fluidized bed reactor.

https://dx.doi.org/10.1021/acs.energyfuels.0c01023
Energy Fuels 2020, 34, 8587−8599

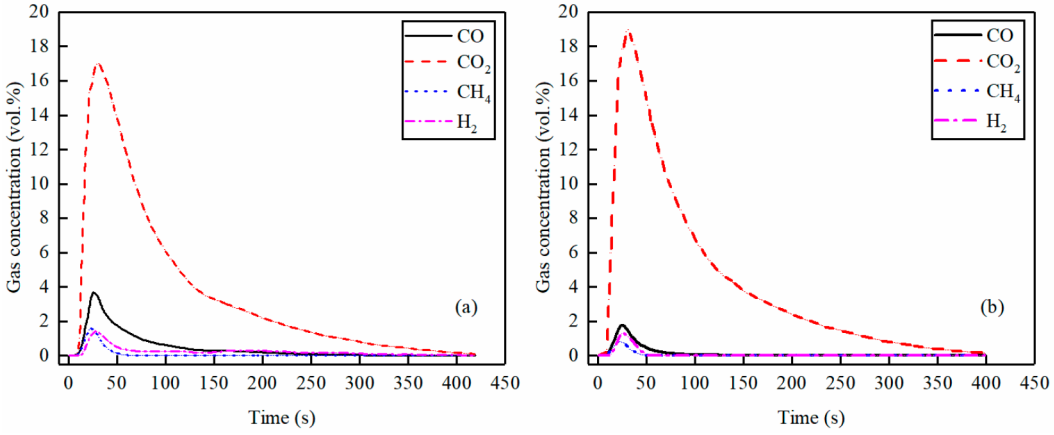

Figure 2. Gas concentration profiles of (a) Fe100 and (b) Cu20Fe80 in the reduction stage. Reaction temperature, 950 °C; oxygen/fuel ratio, 2.5; and fuel, SH bituminous coal.

nitrogen and 50 vol % steam. When the oxygen concentration (oxygen equilibrium partial pressure under a certain temperature) becomes stable, a certain amount of coal is injected into the reactor by a high-pressure pulse of N_2. After the reduction reaction process is completed, air is used to regenerate the reduced OCs. Third, nitrogen is introduced to purge the reactor after each oxidization process. Each test has been repeated 2 or 3 times.

2.4. Data Evaluation. To facilitate the study of the CLC characteristics between OC and coal, the following parameters are defined:

The oxygen/fuel ratio ϕ is calculated as

$$\phi = \frac{n_{O,OC}}{n_{O,coal}} \tag{1}$$

where $n_{O,OC}$ is the molar amount of active oxygen in the OC (considering the process of reducing Fe_2O_3 to Fe_3O_4 and CuO to Cu_2O), and $n_{O,coal}$ is the molar amount of oxygen required for complete combustion of coal.

The outlet gas flow rate during the reduction stage, $F_{out,red}$, is calculated on the basis of the N_2 balance

$$F_{out,red} = \frac{F_{N_2}}{1 - y_{CO} - y_{CO_2} - y_{CH_4} - y_{H_2} - y_{O_2}} \tag{2}$$

where F_{N_2} is the inlet flow rate of N_2; y_{CO_2}, y_{CO}, y_{CH_4}, y_{H_2}, and y_{O_2} are the instantaneous volume fractions of CO_2, CO, CH_4, H_2, and O_2 of the exhaust gas in the reduction stage, respectively.

To further evaluate the reaction process, gas yields (γ_i) of each component (CO_2, CO, CH_4, or H_2) in the exhaust gas and carbon conversion (X_C) of coal during the reduction stage are calculated as

$$\gamma_i = \frac{\int_{t_0}^{t_{total}} (F_{out,red} y_i) dt}{\int_{t_0}^{t_{total}} F_{out,red}(y_{CO} + y_{CO_2} + y_{CH_4}) dt} \tag{3}$$

$$X_C = \frac{\int_{t_0}^{t} F_{out,red}(y_{CO} + y_{CO_2} + y_{CH_4}) dt}{\int_{t_0}^{t_{total}} F_{out,red}(y_{CO} + y_{CO_2} + y_{CH_4}) dt} \tag{4}$$

Here, t_0 and t_{total} represent the time points of the start and end of the reduction stage, respectively, and i represents CO_2, CO, and CH_4, separately.

Especially, $\gamma_{H_2/C}$ can be understood as the ratio of H_2/carbonaceous gases in the exhaust gas.

$$\gamma_{H_2/C} = \frac{\int_{t_0}^{t_{total}} (F_{out,red} y_{H_2}) dt}{\int_{t_0}^{t_{total}} F_{out,red}(y_{CO} + y_{CO_2} + y_{CH_4}) dt} \tag{5}$$

For the average reaction rate of coal throughout the reaction process, the average carbon conversion rate $r_{0.95,C}$ is used as the evaluation standard.

$$r_{0.95,C} = \frac{0.95}{t_{0.95,C} - t_0} \tag{6}$$

Here, $t_{0.95,C}$ represents the time required for carbon conversion to reach 95% during the reduction process.

The carbon conversion rate x_C and instantaneous carbon conversion rate x_{inst} (on the basis of remaining unreacted carbon)[42] are calculated as

$$x_C = \frac{dX_C}{dt} \tag{7}$$

$$x_{inst} = \frac{1}{1 - X_C} \frac{dX_C}{dt} \tag{8}$$

The instantaneous oxygen transfer rate during the reduction process, $x_{O_2,red}(t)$, is determined on the basis of the mass balance of the O atoms in the reactor[47]

$$x_{O_2,red}(t) = M_{O_2}[F_{O_2} + F_{CO_2} + 0.5(F_{CO} + F_{H_2O}) - 0.5F_{H_2O,fed} - 0.5F_{O,coal}] \tag{9}$$

where F_i (including O_2, CO_2, CO, H_2, or CH_4) is the molar gas flow in the exhaust gas during the reduction process, which can be calculated as

$$F_i = \frac{F_{out,red} y_i}{22.4} \tag{10}$$

To measure oxygen leaving with H_2O generating from hydrogen oxidation in the coal, it is assumed that the hydrogen evolution is proportional to the carbon evolution; i.e., the ratio C/H maintains the same value in the gas components as in the coal. Considering the fact that a little methane and hydrogen are detected in the experiment, the H_2O flow rate is calculated as[47]

$$F_{H_2O} = F_{H_2O,fed} + 0.5 f_{H/C}(F_{CO_2} + F_{CO} + F_{CH_4}) - (F_{H_2} + 2F_{CH_4}) \tag{11}$$

where $f_{H/C}$ is the hydrogen/carbon molar ratio in the coal. Similarly, the oxygen evolution from coal is assumed to be proportional to coal evolution. Therefore, the oxygen flow rate coming from coal is calculated as[48]

https://dx.doi.org/10.1021/acs.energyfuels.0c01023
Energy Fuels 2020, 34, 8587−8599

$$F_{O,coal} = f_{O/C}(F_{CO_2} + F_{CO} + F_{CH_4}) \quad (12)$$

where $f_{O/C}$ is the oxygen/carbon molar ratio in the coal.

$F_{out,ox}$ is the outlet gas flow rate at each second during the OC oxidation stage and can be calculated as

$$F_{out,ox} = \frac{0.79F_{air}}{1 - y'_{CO_2} - y'_{O_2}} \quad (13)$$

where F_{air} is the inlet flow rate of air; y'_{CO_2} and y'_{O_2} are the instantaneous volume fractions of CO_2 and O_2 of the exhaust gas in the oxidation stage, respectively.

The combustion efficiency in the reactor, η_{comb}, is used to evaluate the combustion degree of coal in the reactor. It can be calculated as

$$\eta_{comb} = 1 - \frac{\int_{t_0}^{t_{total}} (4F_{CH_4} + F_{CO} + F_{H_2} + 2F'_{CO_2})dt}{\Omega_{coal} m_{coal}} \quad (14)$$

Here, F_{CH_4}, F_{CO}, andF_{H_2} represent the molar gas flows of CH_4, CO, and H_2 in the exhaust gas during the reduction process, respectively; F'_{CO_2} represents the molar gas flow of CO_2 in the exhaust gas during the oxidation process; and Ω_{coal} is the molar amount of oxygen required for complete combustion of coal per unit mass.

Carbon capture efficiency η_{CC} is defined as the ratio of the flow rate of carbon-containing gas converted by fuel during the reduction stage to the total carbon-containing gas flow rate during the reduction and oxidation stages.

$$\eta_{CC} = \frac{\int_{t_0}^{t_{total}} F_{out,red}(y_{CO} + y_{CO_2} + y_{CH_4})dt}{\int_{t_0}^{t_{total}} F_{out,red}(y_{CO} + y_{CO_2} + y_{CH_4})dt + \int_{t_0}^{t_{total}} F_{out,ox} y'_{CO_2} dt} \quad (15)$$

3. RESULTS

3.1. Evaluation of OCs. Figure 2 shows the outlet gas concentration during the reduction stage using Fe100 and Cu20Fe80 as OCs and Shenhua bituminous coal as fuel. The reaction temperature is 950 °C, and the oxygen/fuel ratio is 2.5.

As shown in Figure 2, the CO_2 peak for Cu20Fe80 (18.97 vol %) is higher than that for Fe100 (17 vol %). It can be explained by the fact that more CO and CH_4 are converted by Cu20Fe80 to CO_2, which indicates that the reactivity of Cu20Fe80 is higher than that of Fe100 as a result of the O_2 uncoupling of copper ore or more reactive $CuFe_2O_4$ in Cu20Fe80. The peaks of unconverted CO and CH_4 for Cu20Fe80 are 1.9 and 1.0 vol %, respectively, which are lower than those for Fe100. Within the rapid pyrolysis stage of coal, the small peaks of CO, CH_4, and H_2 appear as a result of the insufficient contact with the OC.[45] The differences among the peak values of combustible gases (CO, CH_4, and H_2) are mainly attributed to the varied reactivity of the OCs toward different gases.[49] During the char gasification stage, H_2 releases gently (shown in panels a and b of Figure 2), which is generated by the char gasification reaction ($C + H_2O = CO + H_2$) and water−gas shift (WGS) reaction ($CO + H_2O = CO_2 + H_2$).[50] Moreover, the unconverted CO concentration shows the same trend. The results clearly indicate that the Cu20Fe80 OC demonstrates higher reactivity, especially under the good mixing of the OC and char gasification products.

The gas yields of CO, CO_2, and CH_4 for Cu20Fe80 and Fe100 during the reduction stage are shown in Figure 3. The yields of CO_2 for Cu20Fe80 and Fe100 are about 96.0 and 86.8%, respectively. The concentrations of unburned combustible gases (CO, H_2, and CH_4) for Cu20Fe80 are lower than those for Fe100. The results also prove that the reactivity of Cu20Fe80 is better than that of Fe100. It should be mentioned that the ratio of H_2 to carbonaceous gases for Fe100 is 5.8%, which is much higher than that for Cu20Fe80. It is due to the limited reactivity of Fe100 to the products of char gasification and WGS reactions. Cu20Fe80 should be a good choice as the OC, and the effects of operational parameters on the CLC performance are further evaluated in the following sections.

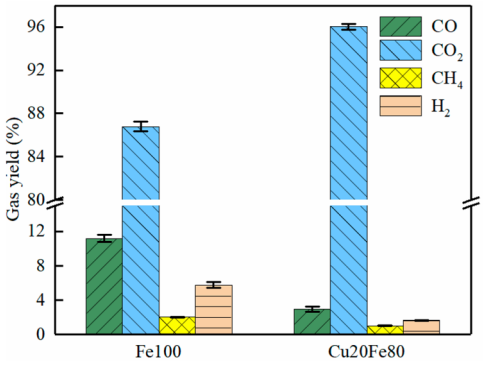

Figure 3. Gas yield of Fe100 and Cu20Fe80 in the reduction stage. Reaction temperature, 950 °C; oxygen/fuel ratio, 2.5; and fuel, SH bituminous coal.

3.2. Effect of the Reaction Temperature. The Cu20Fe80 OC is further tested with Shenhua bituminous coal in the batch fluidized bed reactor under different temperature conditions (850, 900, and 950 °C). The oxygen/fuel ratio is set as 2.5. As known, the conversion of coal is mainly divided into pyrolysis and gasification stages within *in situ* gasification chemical looping combustion (*i*G-CLC): (1) Pyrolysis stage: A large amount of combustible gases will rapidly release in the initial stage, i.e., CO, CH_4, and H_2, and then these gases are oxidized by the OC; (2) Gasification stage: Coal char will be gasified, and then the gasification products are converted by the OC. The instantaneous carbon conversion rate at different temperatures is shown in Figure 4, which clearly demonstrates the two elemental stages. The instantaneous carbon conversion rate at the three temperatures shows a similar trend when carbon conversion (X_C) is smaller than 0.25, which indicates that there is little influence of the temperature on the releasing rate of the pyrolysis products. When the carbon conversion reaches 0.25, the instantaneous carbon conversion rate is decreasing. It is

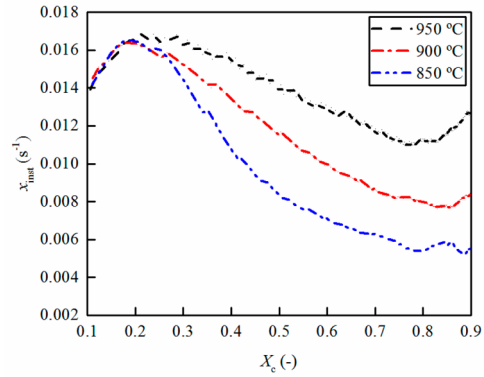

Figure 4. Instantaneous carbon conversion rate versus the carbon conversion of Cu20Fe80 at different temperatures. Oxygen/fuel ratio, 2.5; fuel, SH bituminous coal.

https://dx.doi.org/10.1021/acs.energyfuels.0c01023
Energy Fuels 2020, 34, 8587−8599

mainly because the slow char gasification rate gradually becomes the rate-limiting step. Moreover, with the decreased temperature, the instantaneous carbon conversion rate becomes lower at the same X_C, because a higher temperature is conducive to enhance the char gasification rate. It is worth mentioning that the difference of the CO_2 yield in the three temperatures is relatively small (see Table 5), which indicates that Cu20Fe80 has adequate capacity to combustible gases at the above three temperatures.

Table 5. Effects of Temperatures on the Main Performance Parameters

operation condition			performance parameter			
temperature (°C)	ϕ	coal type	γ_{CO_2} (%)	η_{comb} (%)	η_{CC} (%)	$x_{0.95,C}$ (min^{-1})
850	2.5	SH	95.4	81.2	86.3	0.15
900	2.5	SH	95.9	93.2	98.3	0.18
950	2.5	SH	96.0	95.3	100	0.23

The carbon capture efficiency (η_{CC}) is used to evaluate the conversion degree of solid fuel in the fuel reactor. Figure 5

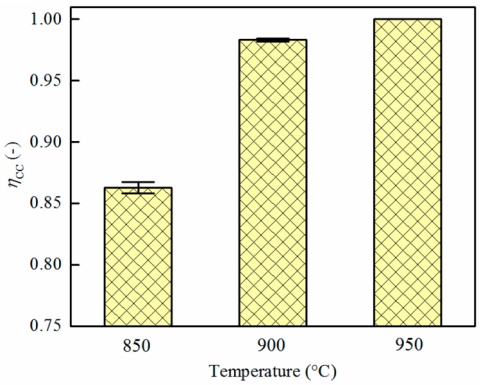

Figure 5. Carbon capture efficiency of Cu20Fe80 at different temperatures. Oxygen/fuel ratio, 2.5; fuel, SH bituminous coal.

shows that the carbon capture efficiency will promote with the increased temperature. The carbon capture efficiency is 86.3% at T = 850 °C, which means that there are still many carbon residues after the reduction stage. At 900 °C, the carbon capture efficiency increases by 12%, indicating that more char is gasified within the reduction stage. The reasons are explained because the higher temperature facilitates the gasification of char and more combustible gases (i.e., H_2 and CO) that can be converted by Cu20Fe80 at a higher temperature, which, in turn, promotes the char gasification reaction ($C + H_2O = H_2 + CO$ and $C + CO_2 = 2CO$). With the temperature increasing to 950 °C, 100% of the carbon capture efficiency is achieved.

As seen from Figure 6a, the average carbon conversion rate increases from 0.15 to 0.23 min^{-1} when the temperature elevates from 850 to 950 °C. The significant decrement of combustion efficiency at 850 °C is mainly due to quite a lot of carbon residues. Although the average carbon conversion rate is higher at 950 °C, the combustion efficiency at 950 °C (η_{comb} = 95.3%) is still slightly higher than that at 900 °C (η_{comb} = 93.2%), which indicates that the *in situ* syngas can be well-converted by the OC and does not exceed the upper limit of the OC oxygen transfer rate under the condition of ϕ = 2.5. A similar phenomenon can be seen in other literature.[9] Figure 6b shows the instantaneous oxygen transfer rate as a function of time. The different peak values provide clear proof that the increase of the temperature will promote the OC reactivity. The increased OC reactivity then contributes to quite a high combustion efficiency at 900−950 °C. The total amount of oxygen donation from Cu20Fe80 is 0.43 g at 950 °C, 0.42 g at 900 °C, and 0.36 g at 850 °C. The difference of the oxygen donation amount is related to different char gasification rates and reactivities of OC and, therefore, different char conversions and finally different carbon residues at different temperatures.

Table 5 gathers these important parameters (CO_2 yield γ_{CO_2}, combustion efficiency η_{comb}, carbon capture efficiency η_{CC}, and average carbon conversion rate $x_{0.95,C}$) at different temperatures (ϕ = 2.5 and SH bituminous coal). All of the parameters present an upward trend with the increase of the temperature. As seen from Table 5, the temperature is a vital factor affecting the average carbon conversion rate, which was also proven by our previous work.[42] The decrement of combustion efficiency is mainly ascribed to more carbon residues at a relatively low temperature. In summary, 950 °C is a more suitable temperature and Cu20Fe80 OC exhibits better performance

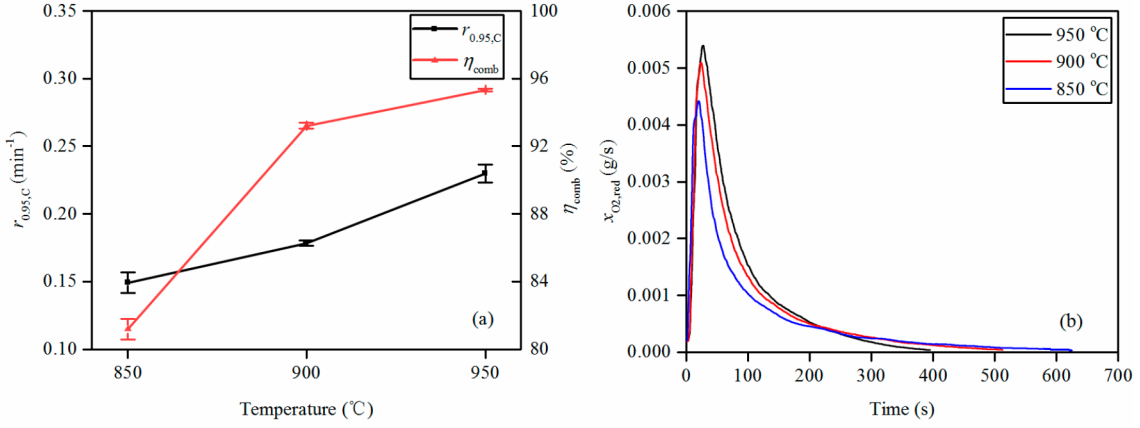

Figure 6. (a) Average carbon conversion rate and combustion efficiency and (b) instantaneous oxygen transfer rate versus time of Cu20Fe80 at different temperatures. Oxygen/fuel ratio, 2.5; fuel, SH bituminous coal.

https://dx.doi.org/10.1021/acs.energyfuels.0c01023
Energy Fuels 2020, 34, 8587−8599

to achieve a complete conversion of carbon and high average carbon conversion rate.

3.3. Effect of the Oxygen/Fuel Ratio. Figure 7 illustrates the yields of CO, CO_2, CH_4, and H_2 under different oxygen/fuel ratios (ϕ = 1.5, 2.0, and 2.5) using Cu20Fe80 as the OC and SH bituminous coal as the solid fuel. The temperature is maintained at 950 °C, and the fluidized gas is 50 vol % steam + 50 vol % N_2. The change of the oxygen/fuel ratio is achieved by adjusting the coal mass fed at each test. It can be seen that quite high CO_2 yields are achieved at the three cases. Even though the oxygen/fuel ratio is low to 1.5, the CO_2 yield is about 94.6%. When it further increases to 2.5, the CO_2 yield increases by 1.4%. In addition, the yield of unburned gases shows a downward trend with the increase of the oxygen/fuel ratio. The reaction time is defined as the start of the initial increase of the carbon-containing gas and the end of CO_2 dropping to 0.15% during the reduction stage. There is no obvious difference of the reaction time when the oxygen/fuel ratio is 2.0 and 2.5. However, the reaction time sharply increases to 461 s at ϕ = 1.5. The reason for the rapid increase of the reaction time is that the OC is unable to react in time with all combustible gases as a result of the increase of coal mass, and then these combustible gases may inhibit the char gasification more or less. The results indicate that the sufficient OC can accelerate the char gasification rate as a result of the consumption of H_2 and CO.

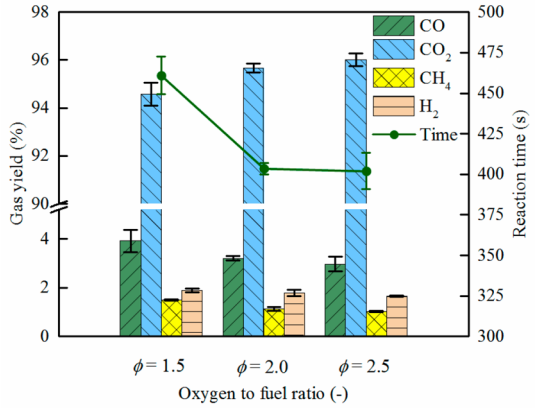

Figure 7. Gas yield and reaction time of Cu20Fe80 with different oxygen/fuel ratios. Reaction temperature, 950 °C; fuel, SH bituminous coal.

Table 6 shows the parameters (CO_2 yield γ_{CO_2}, combustion efficiency η_{comb}, carbon capture efficiency η_{CC}, and average carbon conversion rate $x_{0.95,C}$) for different oxygen/fuel ratios (T = 950 °C and SH bituminous coal). From Table 6, all of the performance parameters show an upward trend with the increase of the oxygen/fuel ratio, which is certainly caused by the increase of active oxygen in the reaction system. Although the high oxygen/fuel ratio can improve the combustion performance, the bed inventory will increase, which then burdens higher operation cost. Therefore, a suitable value of the oxygen/fuel ratio should be attained. On the other side, it is noticed that the influence of the oxygen/fuel ratio on these performance parameters is not so obvious. Therefore, it is conjectured that a relatively small oxygen/fuel ratio in the range of 1.1−1.5 can be adopted in an interconnected fluidized bed reactor. Considering the situation of gas−solid mixing in the batch fluidized bed, the value of ϕ in the work is higher than that in the continuously operated CLC units.

Table 6. Effects of Oxygen/Fuel Ratios on the Main Performance Parameters

operation condition			performance parameter			
temperature (°C)	ϕ	coal type	γ_{CO_2} (%)	η_{comb} (%)	η_{CC} (%)	$x_{0.95,C}$ (min^{-1})
950	1.5	SH	94.6	93.6	100	0.21
950	2.0	SH	95.7	95.1	100	0.23
950	2.5	SH	96.0	95.3	100	0.23

3.4. Effect of the Coal Rank. To explore the matching characteristics between different coals and the Cu20Fe80 OC, the *i*G-CLC performance with three typical coal ranks is also evaluated. The temperature is kept at 950 °C; the oxygen/fuel ratio is 2.0; and 50 vol % H_2O + 50 vol % N_2 is used as the fluidizing gases.

Panels a and b of Figure 8 present the carbon conversion rate and instantaneous carbon conversion rate of Cu20Fe80 with CF lignite, SH bituminous coal, and SX anthracite. As presented in Figure 8a, CF lignite can be completely converted within 300 s and the time for SH bituminous coal takes about 400 s, while the time for SX anthracite takes about 650 s. Accordingly, the instantaneous carbon conversion rate (Figure 8b) of CF lignite is the highest, followed by SH bituminous coal and SX anthracite. The main reason is that lignite and bituminous coal are more easily gasified by H_2O. Thus, the main limitation to the carbon conversion rate is the char gasification rate in *i*G-CLC of coal[45] rather than the reactivity (or oxygen transfer rate) of the Cu20Fe80 OC.

Table 7 presents the important parameters (CO_2 yield γ_{CO_2}, combustion efficiency η_{comb}, carbon capture efficiency η_{CC}, and average carbon conversion rate $x_{0.95,C}$) with different coal ranks (T = 950 °C and ϕ = 2.0). An order of the average carbon conversion rate is listed as lignite > bituminous coal > anthracite. The reason can be explained in two aspects: (1) the volatile content of low-rank coals is higher, and the combustion of more volatiles lead to the rise of the local temperature, which makes a contribution to a faster conversion of coal char, and (2) the gasification of low-rank coal char is easier than that of high-rank coal char.[51] The fast conversion rate of low-rank coal and bypassing of many combustible gases (from the early pyrolysis) result in the decrement of combustion efficiency.

3.5. Stability Assessment of Cu20Fe80. To further study the stability of Cu20Fe80 during the CLC process, 10 redox cycles are performed for the same batch of Cu20Fe80 OC after the above tests. Figure 9 shows the gas yield and concentrations of CO_2, CO, CH_4, and H_2 in the 10 cycles (with SH bituminous coal). For all tests, the reaction temperature is maintained at 950 °C, the fluidization agent is 50 vol % H_2O + 50 vol % N_2, and the oxygen/fuel ratio is kept at 2.5. The CO_2 yield remains at a high level during the 10 cycles, which are all about 96%. Unreacted gases are kept stable at a low level. Thus, the good reactivity of Cu20Fe80 maintains well within the whole tests, and no significant deactivation phenomenon occurs in the last 10 cycles.

3.6. Characterization of OCs. Figure 10 shows the XRD patterns (X'Pert PRO, Netherlands) of the fresh, oxidation, and reduction states of Fe100 and Cu20Fe80 after cyclic tests with SH bituminous coal, separately. It can be seen from

https://dx.doi.org/10.1021/acs.energyfuels.0c01023
Energy Fuels 2020, 34, 8587−8599

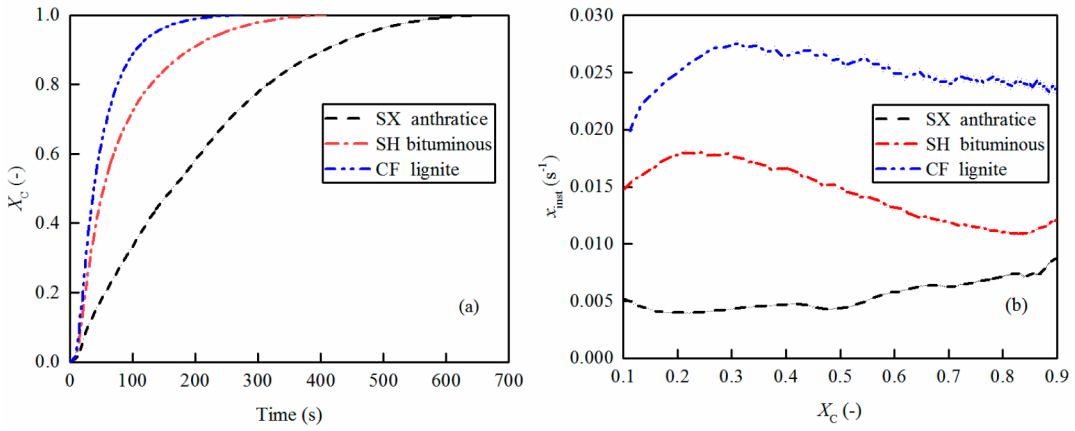

Figure 8. (a) Carbon conversion rate versus time and (b) instantaneous carbon conversion rate versus carbon conversion with different coal ranks. Reaction temperature, 950 °C; oxygen/fuel ratio, 2.0.

Table 7. Effects of Coal Ranks on the Main Performance Parameters

operation condition			performance parameter			
temperature (°C)	ϕ	coal type	γ_{CO_2} (%)	η_{comb} (%)	η_{CC} (%)	$x_{0.95,C}$ (min^{-1})
950	2.0	CF	95.1	94.9	100	0.39
950	2.0	SH	95.7	95.1	100	0.23
950	2.0	SX	95.8	97.7	100	0.12

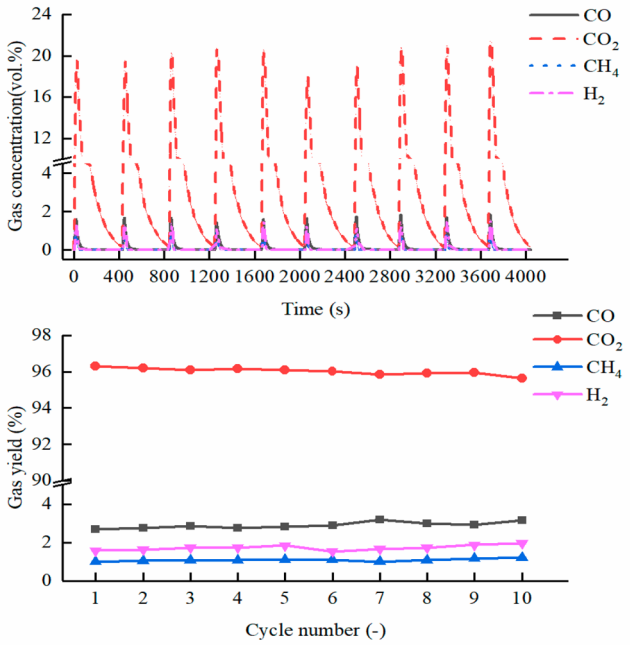

Figure 9. Gas concentration and yield of Cu20Fe80 during 10 cycles. Reaction temperature, 950 °C; oxygen/fuel ratio, 2.5; and fuel, SH bituminous coal.

Figure 10 that the active component of Fe100 is mainly Fe_2O_3. CuO diffraction peaks are not detected in the fresh and oxidized Cu20Fe80 sample, which is probably due to the reaction between Fe_2O_3 and CuO to generate $CuFe_2O_4$.[45] Because the amount of lattice oxygen in the fluidized bed is more than that of required oxygen for full conversion of coal, a small amount of Fe_2O_3 is detected in the reduction state of both Fe100 and Cu20Fe80.

The morphology and structure of Fe100 and Cu20Fe80 samples are characterized by ESEM (FEI Quanta 200) with an acceleration voltage of 20.0 kV. In panels a and d of Figure 11, the spherical and porous OCs can be obtained by the spray drying method for fresh Fe100 and Cu20Fe80. The spherical structure is maintained well after the redox cycles, which is beneficial to keep the good fluidization and enhance the lifetime of the OC. In panels b and c as well as panels e and f of Figure 11, no obvious sintering is observed on the surface of the OC particles for Fe100 and Cu20Fe80. The used samples have a rougher surface and more abundant pore structure for used Cu20Fe80 than Fe100. The BET results also indicate that the specific surface area of used Cu20Fe80 is about 2.5 times to that of the fresh sample, which is 0.2411 m^2/g. It can be explained by the fact that $CuFe_2O_4$ can release gaseous oxygen, which develops more pores and channels.

The cross-section SEM−EDS analysis of fresh Cu20Fe80 and used Cu20Fe80 after cyclic redox is performed to investigate the distribution of elements (Cu and Fe) in Cu20Fe80, as shown in Figure 12. The Fe element is always uniformly distributed inside both fresh and used samples, which acts as a framework for the particles. Moreover, the Cu element is partially lost and better uniformly distributes in the used sample (as shown in Figure 12f). However, as shown in Figure 13, the intensity of the diffraction peak of the Cu element in the cross section after the cyclic redox does not decrease obviously compared to the fresh sample, which indicates that the relative content of the Cu element has hardly decreased. Detected C comes from the carbon coating (to enhance the conductivity of the particles) before the ESEM test.

4. DISCUSSION

4.1. Comparison among Three Kinds of Bi-ore OCs.

Bi- or multi-active phase OC, as a superior choice, can integrate the advantages of different metal oxides. Considering that hematite is quite cheap but also less reactive in CLC, while copper ore has high oxygen carrying capacity and good reactivity but suffers from sintering at a high temperature, the composite OCs based on hematite and copper ore were studied systematically in our group. The cost of OCs can be reduced using ores with great price advantage instead of synthetic chemicals. Yang et al.[20] first proposed this idea, using mechanically mixed copper ore and hematite as the OC

https://dx.doi.org/10.1021/acs.energyfuels.0c01023
Energy Fuels 2020, 34, 8587−8599

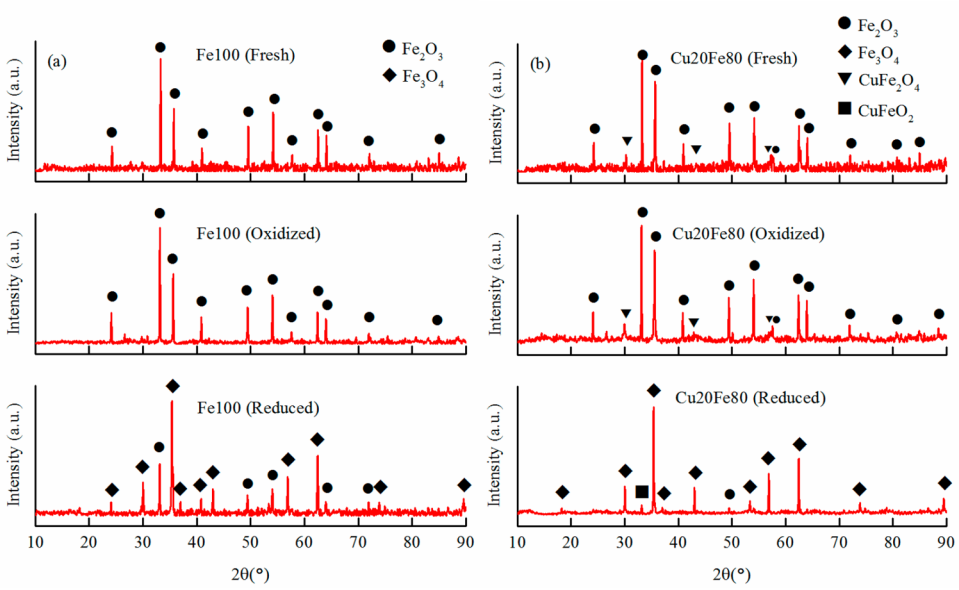

Figure 10. XRD patterns of (a) Fe100 and (b) Cu20Fe80 in the fresh, oxidized, and reduced (under T = 950 °C, ϕ = 2.5, and SH bituminous coal) states.

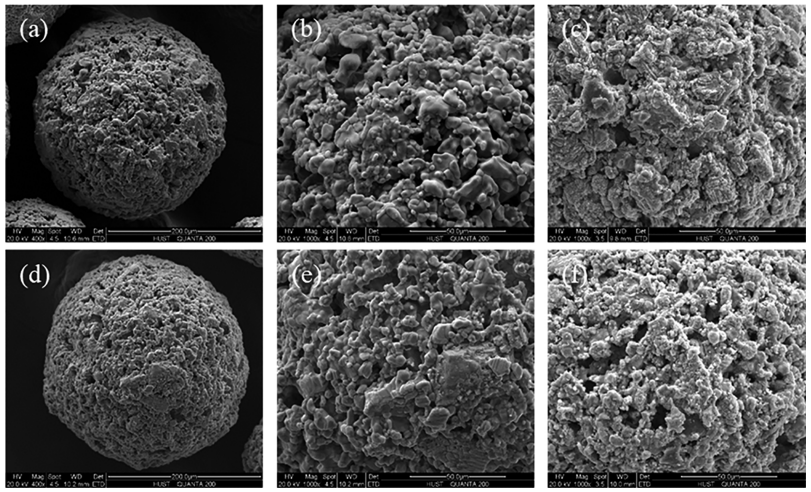

Figure 11. ESEM images of Fe100: (a) fresh sample at 500×, (b) fresh sample at 1000×, and (c) used sample at 1000× and Cu20Fe80: (d) fresh sample at 500×, (e) fresh sample at 1000×, and (f) used sample at 1000×.

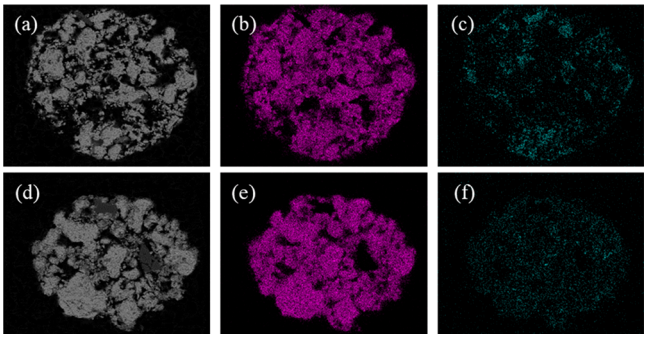

Figure 12. SEM−EDS images of fresh Cu20Fe80: (a) cross section, (b) Fe element distribution, and (c) Cu element distribution and used Cu20Fe80: (d) cross section, (e) Fe element distribution, and (f) Cu element distribution.

(named M−Cu−Fe). The results demonstrated that the copper ore can be more efficiently used when the mixing ratio of copper ore maintained 10−20 wt %; that is, the synergistic effect between hematite and copper ore worked best at this ratio. Further tests of DTA showed that thermal neutrality in the fuel reactor can be achieved when the copper ore ratio was 20 wt %.

To avoid the segregation phenomenon in the reactor as a result of the different densities of mechanically mixed hematite and copper ore, Tian et al.[45] used 20 wt % cement as the binding medium to bond fine powders of hematite and copper ore into a single particle (named C−Cu−Fe). The synergistic effect was also observed in thermogravimetric analysis (TGA) tests when the hematite/copper ore ratio was 80/20 wt %.

However, for the cement bonding method, the mixed slurries of materials need to dry for several days at room temperature to obtain the high hardness of bulk products. When turning to large-scale preparation, the defect of a long preparation period becomes particularly obvious. The spray drying method has been widely used in industry for its advantage of high-efficiency granulation and, factually, has

https://dx.doi.org/10.1021/acs.energyfuels.0c01023
Energy Fuels 2020, 34, 8587−8599

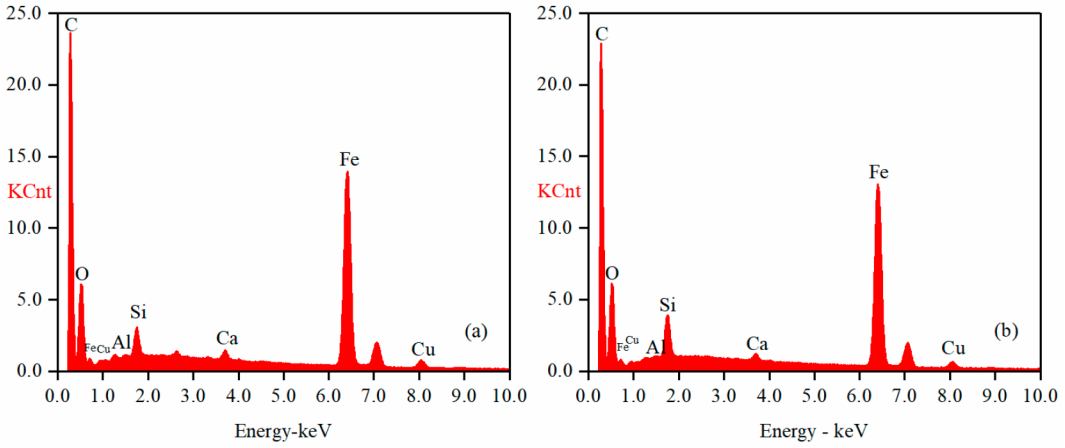

Figure 13. Cross-section SEM−EDS analysis of (a) fresh Cu20Fe80 and (b) used Cu20Fe80.

Table 8. Comparison of OCs Prepared by Three Different Methods

OC	active phase	fuel type	performance
M−Cu−Fe	CuO, Fe_2O_3, and $CuFe_2O_4$	syngas and coals	79% CO_2 yield and average instantaneous carbon conversion rate of 15.9%/min with GP anthracite when T = 950 °C and ϕ = 1.0
C−Cu−Fe	CuO, Fe_2O_3, and $CuFe_2O_4$	syngas and coals	more than 94% CO_2 yield with SL lignite when T = 950 °C and $\phi \geq 2.0$; SL lignite was completely converted within 400 s when T = 950 °C and ϕ = 2.0; reactivity maintained well within 30 cycles
S−Cu−Fe	$CuFe_2O_4$ and Fe_2O_3	coals	maximum average carbon conversion rate of 23%/min with SH bituminous coal; CF lignite is completely converted within 300 s when T = 950 °C and ϕ = 2.0; over 94% CO_2 yield with SH bituminous coal when T = 950 °C and $\phi \geq 1.5$

been adopted for OC preparation. The use of ores as raw material in spray drying is relatively rare. Only manganese ore as a raw material of the spray drying method has been studied;[36] however, using copper ore and hematite as raw materials of spray drying granulation has not been published. Therefore, the spray drying method is introduced in this work to prepare the bi-ore OC (named S−Cu−Fe). The ratio of copper ore/hematite is also selected as 20:80 wt % to achieve the synergistic effect and thermal neutrality of the fuel reactor. Table 8 gathers and compares the characteristics of M−Cu−Fe,[20] C−Cu−Fe,[45] and S−Cu−Fe. As seen from Table 8, the active phase of CuO is not be found in S−Cu−Fe as a result of the higher calcination temperature than the other two OCs. S−Cu−Fe is at least as reactive as the other two OCs. In addition, the crushing strength of S−Cu−Fe is 1.7 ± 0.2 N, which probably satisfies the requirement of fluidized bed reactor application. The bi-ore OC prepared by spray drying can not only solve the segregation phenomenon caused by different densities of particles in the mechanical mixing method but also address the problem of the long preparation period in the cement bonding method. In view of the unique advantages (high efficiency, scalable production, etc.) of spray drying, it will be the promising method for large-scale preparation of OCs.

4.2. Economical Evaluation. The cost of raw materials of OC is a common concern in the CLC community. Table 9 shows the raw material cost of the minerals (including refined copper ore and natural hematite), mechanical mixed bi-ore OC[20] (M−Cu−Fe), cement bonded bi-ore OC[45] (C−Cu−Fe), and spray-drying-derived bi-ore OC (S−Cu−Fe). The estimated costs of OCs are based on providing per kilogram active oxygen. It can be seen from Table 9 that the prices of C−Cu−Fe and S−Cu−Fe are slightly more expensive than that of M−Cu−Fe as a result of the additives of cement in C−Cu−Fe and binder & dispersant in S−Cu−Fe. Moreover, the difference of the raw material costs between C−Cu−Fe and S−Cu−Fe is relatively small. The unit price of these OCs is estimated to be $1.6/kg for copper ore, $0.5/kg for hematite, $0.72/kg for M−Cu−Fe, $0.62/kg for C−Cu−Fe, and $0.79/kg for S−Cu−Fe. In addition, the unit price of Fe100 OC prepared by spray drying is $0.57/kg. However, it is worth noting that the equipment investment required for spray drying is expensive. Therefore, if it is just for laboratory-scale preparation of OCs, the mechanical mixing method and cement bonding method can be the favorite choice as a result of their characteristics of simplicity and convenience. Nevertheless, when it comes to large-scale preparation, the OC prepared by the spray drying method is undoubtedly attractive.

5. CONCLUSION

In this work, fine powders of hematite and copper ore (<100 μm) are used as raw materials for the preparation of composite OC. Fe100 (only hematite) and Cu20Fe80 (copper ore, 20 wt %; hematite, 80 wt %) are successfully prepared by the spray drying granulation method.

The performance of Fe100 and Cu20Fe80 is evaluated in a batch fluidized bed reactor at different temperatures, oxygen/fuel ratios, and various coal ranks. The results show that the reactivity of Cu20Fe80 is no doubt better than that of Fe100. When using Cu20Fe80 as the OC, the instantaneous carbon conversion rates exhibit a similar trend within the early coal pyrolysis process at different reaction temperatures (850, 900, and 950 °C). Moreover, the temperature shows a promotion on the instantaneous carbon conversion rate during the char gasification process. The temperature of 950 °C is a suitable reaction temperature with a high average carbon conversion rate and carbon capture efficiency. There is an over 94% CO_2 yield with SH bituminous coal when T = 950 °C and $\phi \geq 1.5$.

https://dx.doi.org/10.1021/acs.energyfuels.0c01023
Energy Fuels 2020, 34, 8587−8599

Table 9. Raw Material Costs of Fresh OCs

chemical	copper ore ($/kg [O])	hematite ($/kg [O])	M−Cu−Fe ($/kg [O])	C−Cu−Fe ($/kg [O])	S−Cu−Fe ($/kg [O])
copper ore	1.6 ($/kg) × 18.6 (kg/kg [O])		1.6 ($/kg) × 5.72 (kg/kg [O])	1.6 ($/kg) × 5.72 (kg/kg [O])	1.6 ($/kg) × 5.72 (kg/kg [O])
hematite		0.5 ($/kg) × 33.1 (kg/kg [O])	0.5 ($/kg) × 22.9 (kg/kg [O])	0.5 ($/kg) × 22.9 (kg/kg [O])	0.5 ($/kg) × 22.9 (kg/kg [O])
cement[a]				0.22 ($/kg) × 7.37 (kg/kg [O])	
binder[b]					2.86 ($/kg) × 0.47 (kg/kg [O])
dispersant[c]					2.14 ($/kg) × 0.29 (kg/kg [O])
OC cost	29.76	16.55	20.60	22.17	22.54

[a]https://topic2012.en.made-in-china.com/product/nvuJjAYBsmcV/China-Refractory-Cement-High-Alumina-Cement-for-Refractory-CA-.html. [b]https://detail.1688.com/offer/565378723980.html. [c]https://detail.1688.com/offer/610916034272.html.

Moreover, CF lignite and SH bituminous coal can be fully reacted within 400 s, while SX anthracite takes a longer time, which is related to the char gasification characteristics of different coal ranks.

With respect to the durability of the Cu20Fe80 OC, the CO_2 gas yield can be maintained at about 96% during >10 cyclic redox tests, which verifies the good stability of Cu20Fe80. No obvious sintering is found from the ESEM images of the used particles, and the distribution of the Cu element is more uniform after the cyclic tests through the EDS result. The estimated cost of raw materials of the spray-drying-derived bi-ore OC (S−Cu−Fe) is 22.54 $/kg [O], which is slightly higher than that of the cement-bonded bi-ore OC (C−Cu−Fe, 22.17 $/kg [O]). There is a price difference between S−Cu−Fe and mechanically mixed bi-ore OC (M−Cu−Fe, 20.60 $/kg [O]) as a result of additives of binder and dispersant. The Cu20Fe80 OC exhibits good reactivity toward coals on the whole, and it is not inferior to that of C−Cu−Fe and M−Cu−Fe. Considering that the raw materials of the Cu20Fe80 OC are relatively cheap and the preparation process is able to scale up, together with the outstanding comprehensive performance, the Cu20Fe80 OC prepared by the spray drying method could be a promising OC candidate in the coal-derived CLC process.

However, we realize that the preparation processes of the spray drying granulation method deserve further optimization [including the calcination processes (here in a high-temperature muffle furnace)] and further scaling-up (here only several kilograms were prepared for each batch). Also, the prepared OC should be further evaluated in terms of attrition/fragmentation, agglomeration, and sintering in a long-term test (preferably in a continuously operated CLC unit).

AUTHOR INFORMATION

Corresponding Author

Haibo Zhao − *State Key Laboratory of Coal Combustion, School of Energy and Power Engineering, Huazhong University of Science and Technology, Wuhan, Hubei 430074, People's Republic of China;* orcid.org/0000-0002-2693-4499; Phone: +86-27-87544779-8208; Email: hzhao@mail.hust.edu.cn; Fax: +86-27-87545526

Authors

Zhao Su − *State Key Laboratory of Coal Combustion, School of Energy and Power Engineering, Huazhong University of Science and Technology, Wuhan, Hubei 430074, People's Republic of China*

Yanan Wang − *State Key Laboratory of Coal Combustion, School of Energy and Power Engineering, Huazhong University of Science and Technology, Wuhan, Hubei 430074, People's Republic of China*

Han Du − *State Key Laboratory of Coal Combustion, School of Energy and Power Engineering, Huazhong University of Science and Technology, Wuhan, Hubei 430074, People's Republic of China*

Jinchen Ma − *State Key Laboratory of Coal Combustion, School of Energy and Power Engineering, Huazhong University of Science and Technology, Wuhan, Hubei 430074, People's Republic of China*

Ying Zheng − *State Key Laboratory of Coal Combustion, School of Energy and Power Engineering, Huazhong University of Science and Technology, Wuhan, Hubei 430074, People's Republic of China*

https://dx.doi.org/10.1021/acs.energyfuels.0c01023
Energy Fuels 2020, 34, 8587−8599

Complete contact information is available at:
https://pubs.acs.org/10.1021/acs.energyfuels.0c01023

Notes

The authors declare no competing financial interest.

■ ACKNOWLEDGMENTS

This work was supported by the National Key R&D Program of China (2018YFB0605402). The staff from the Analytical and Testing Center at the Huazhong University of Science and Technology are appreciated for their related experimental analysis.

■ REFERENCES

(1) Zhao, X.; Cai, Q.; Ma, C.; Hu, Y.; Luo, K.; Li, W. Economic Evaluation of Environmental Externalities in China's Coal-Fired Power Generation. *Energy Policy* **2017**, *102*, 307−317.
(2) Richter, H. J.; Knoche, K. F. Reversibility of Combustion Process, Efficiency and Costing, Second Law Analysis of Process. *ACS Symp. Ser.* **1983**, *235*, 71−86.
(3) Ishida, M.; Jin, H. A New Advanced Power-Generation System Using Chemical-Looping Combustion. *Energy* **1994**, *19* (4), 415−422.
(4) Ishida, M.; Jin, H.; Okamoto, T. A Fundamental Study of a New Kind of Medium Material for Chemical-Looping Combustion. *Energy Fuels* **1996**, *10* (4), 958−963.
(5) Ohlemüller, P.; Reitz, M.; Ströhle, J.; Epple, B. Investigation of Chemical Looping Combustion of Natural Gas at 1 MW_{th} Scale. *Proc. Combust. Inst.* **2019**, *37* (4), 4353−4360.
(6) Ströhle, J.; Orth, M.; Epple, B. Chemical Looping Combustion of Hard Coal in a 1 MW_{th} Pilot Plant Using Ilmenite as Oxygen Carrier. *Appl. Energy* **2015**, *157*, 288−294.
(7) Abad, A.; Pérez-Vega, R.; de Diego, L. F.; García-Labiano, F.; Gayán, P.; Adánez, J. Design and Operation of a 50 kW_{th} Chemical Looping Combustion (CLC) Unit for Solid Fuels. *Appl. Energy* **2015**, *157*, 295−303.
(8) Linderholm, C.; Lyngfelt, A.; Cuadrat, A.; Jerndal, E. Chemical-Looping Combustion of Solid Fuels—Operation in a 10 kW Unit with Two Fuels, above-Bed and in-Bed Fuel Feed and Two Oxygen Carriers, Manganese Ore and Ilmenite. *Fuel* **2012**, *102*, 808−822.
(9) Ma, J.; Tian, X.; Wang, C.; Chen, X.; Zhao, H. Performance of a 50 kW_{th} Coal-Fuelled Chemical Looping Combustor. *Int. J. Greenhouse Gas Control* **2018**, *75*, 98−106.
(10) Song, T.; Wu, J.; Zhang, H.; Shen, L. Characterization of an Australia Hematite Oxygen Carrier in Chemical Looping Combustion with Coal. *Int. J. Greenhouse Gas Control* **2012**, *11*, 326−336.
(11) Tian, H.; Siriwardane, R.; Simonyi, T.; Poston, J. Natural Ores as Oxygen Carriers in Chemical Looping Combustion. *Energy Fuels* **2013**, *27* (8), 4108−4118.
(12) Mei, D.; Mendiara, T.; Abad, A.; De Diego, L. F.; García-Labiano, F.; Gayán, P.; Adánez, J.; Zhao, H. Evaluation of Manganese Minerals for Chemical Looping Combustion. *Energy Fuels* **2015**, *29* (10), 6605−6615.
(13) Schmitz, M.; Linderholm, C. Chemical Looping Combustion of Biomass in 10- and 100-kW Pilots—Analysis of Conversion and Lifetime Using a Sintered Manganese Ore. *Fuel* **2018**, *231*, 73−84.
(14) Linderholm, C.; Lyngfelt, A.; Dueso, C. Chemical-Looping Combustion of Solid Fuels in a 10 kW Reactor System Using Natural Minerals as Oxygen Carrier. *Energy Procedia* **2013**, *37*, 598−607.
(15) Shen, L.; Wu, J.; Gao, Z.; Xiao, J. Characterization of Chemical Looping Combustion of Coal in a 1 kW_{th} Reactor with a Nickel-Based Oxygen Carrier. *Combust. Flame* **2010**, *157* (5), 934−942.
(16) Penthor, S.; Zerobin, F.; Mayer, K.; Pröll, T.; Hofbauer, H. Investigation of the Performance of a Copper Based Oxygen Carrier for Chemical Looping Combustion in a 120 kW Pilot Plant for Gaseous Fuels. *Appl. Energy* **2015**, *145*, 52−59.
(17) Zafar, Q.; Abad, A.; Mattisson, T.; Gevert, B. Reaction Kinetics of Freeze-Granulated $NiO/MgAl_2O_4$ Oxygen Carrier Particles for Chemical-Looping Combustion. *Energy Fuels* **2007**, *21* (2), 610−618.
(18) Zhang, Y.; Liu, F.; Chen, L.; Han, C.; Richburg, L. R.; Neathery, J. K.; Liu, K. Investigation of the Water Vapor Influence on the Performance of Iron-, Copper-, and Nickel-Based Oxygen Carriers for Chemical Looping Combustion. *Energy Fuels* **2013**, *27* (9), 5341−5351.
(19) Adánez, J.; García-Labiano, F.; de Diego, L. F.; Gayán, P.; Abad, A.; Celaya, J. Development of Oxygen Carriers for Chemical-Looping Combustion. *Carbon Dioxide Capture Storage Deep Geol. Form.* **2005**, 587−604.
(20) Yang, W.; Zhao, H.; Wang, K.; Zheng, C. Synergistic Effects of Mixtures of Iron Ores and Copper Ores as Oxygen Carriers in Chemical-Looping Combustion. *Proc. Combust. Inst.* **2015**, *35* (3), 2811−2818.
(21) Costa, T. R.; Gayán, P.; Abad, A.; García-Labiano, F.; de Diego, L. F.; Melo, D. M. A.; Adánez, J. Mn-Based Oxygen Carriers Prepared by Impregnation for Chemical Looping Combustion with Diverse Fuels. *Fuel Process. Technol.* **2018**, *178* (May), 236−250.
(22) de Diego, L. F.; Gayán, P.; García-Labiano, F.; Celaya, J.; Abad, A.; Adánez, J. Impregnated CuO/Al_2O_3 Oxygen Carriers for Chemical-Looping Combustion: Avoiding Fluidized Bed Agglomeration. *Energy Fuels* **2005**, *19* (5), 1850−1856.
(23) Guo, L.; Zhao, H.; Ma, J.; Mei, D.; Zheng, C. Comparison of Large-Scale Production Methods of Fe_2O_3/Al_2O_3 Oxygen Carriers for Chemical-Looping Combustion. *Chem. Eng. Technol.* **2014**, *37* (7), 1211−1219.
(24) Baek, J. I.; Ryu, C. K.; Eom, T. H.; Lee, J. B.; Jeon, W. S.; Yi, J. Chemical-Looping Combustion of Syngas by Means of Spray-Dried NiO Oxygen Carrier. *Korean J. Chem. Eng.* **2011**, *28* (11), 2211−2217.
(25) Azimi, G.; Mattisson, T.; Leion, H.; Rydén, M.; Lyngfelt, A. Comprehensive Study of Mn-Fe-Al Oxygen-Carriers for Chemical-Looping with Oxygen Uncoupling (CLOU). *Int. J. Greenhouse Gas Control* **2015**, *34*, 12−24.
(26) De Vos, Y.; Jacobs, M.; Van Driessche, I.; Van Der Voort, P.; Snijkers, F.; Verberckmoes, A. Processing and Characterization of Fe-Based Oxygen Carriers for Chemical Looping for Hydrogen Production. *Int. J. Greenhouse Gas Control* **2018**, *70*, 12−21.
(27) De Vos, Y.; Jacobs, M.; Van Der Voort, P.; Van Driessche, I.; Snijkers, F.; Verberckmoes, A. Sustainable Iron-Based Oxygen Carriers for Chemical Looping for Hydrogen Generation. *Int. J. Hydrogen Energy* **2019**, *44* (3), 1374−1391.
(28) Jerndal, E.; Mattisson, T.; Thijs, I.; Snijkers, F.; Lyngfelt, A. Investigation of $NiO/NiAl_2O_4$ Oxygen Carriers for Chemical-Looping Combustion Produced by Spray-Drying. *Int. J. Greenhouse Gas Control* **2010**, *4* (1), 23−35.
(29) Baek, J. I.; Ryu, C. K.; Ryu, J.; Kim, J. W.; Eom, T. H.; Lee, J. B.; Yi, J. Performance Comparison of Spray-Dried Oxygen Carriers: The Effect of NiO and Pseudoboehmite Content in Raw Materials. *Energy Fuels* **2010**, *24* (10), 5757−5764.
(30) Baek, J. I.; Ryu, C. K.; Lee, J. H.; Eom, T. H.; Lee, J. B.; Ryu, H. J.; Ryu, J.; Yi, J. The Effects of Using Structurally Less-Stable Raw Materials for the Support of a Spray-Dried Oxygen Carrier with High NiO Content. *Fuel* **2012**, *102*, 106−114.
(31) Adánez-Rubio, I.; Abad, A.; Gayán, P.; García-Labiano, F.; De Diego, L. F.; Adánez, J. The Fate of Sulphur in the Cu-Based Chemical Looping with Oxygen Uncoupling (CLOU) Process. *Appl. Energy* **2014**, *113*, 1855−1862.
(32) Adánez-Rubio, I.; Arjmand, M.; Leion, H.; Gayán, P.; Abad, A.; Mattisson, T.; Lyngfelt, A. Investigation of Combined Supports for Cu-Based Oxygen Carriers for Chemical-Looping with Oxygen Uncoupling (CLOU). *Energy Fuels* **2013**, *27* (7), 3918−3927.
(33) Frick, V.; Rydén, M.; Leion, H.; Mattisson, T.; Lyngfelt, A. Screening of Supported and Unsupported Mn-Si Oxygen Carriers for CLOU (Chemical-Looping with Oxygen Uncoupling). *Energy* **2015**, *93*, 544−554.

(34) Pérez-Vega, R.; Abad, A.; Izquierdo, M. T.; Gayán, P.; de Diego, L. F.; Adánez, J. Evaluation of Mn-Fe Mixed Oxide Doped with TiO_2 for the Combustion with CO_2 Capture by Chemical Looping Assisted by Oxygen Uncoupling. *Appl. Energy* **2019**, *237*, 822−835.
(35) Jacobs, M.; van der Kolk, T.; Albertsen, K.; Mattisson, T.; Lyngfelt, A.; Snijkers, F. Synthesis and Upscaling of Perovskite Mn-Based Oxygen Carrier by Industrial Spray Drying Route. *Int. J. Greenhouse Gas Control* **2018**, *70*, 68−75.
(36) Mattisson, T.; Linderholm, C.; Jerndal, E.; Lyngfelt, A. Enhanced Performance of Manganese Ore as Oxygen Carrier for Chemical-Looping with Oxygen Uncoupling (CLOU) by Combination with $Ca(OH)_2$ through Spray-Drying. *J. Environ. Chem. Eng.* **2016**, *4* (4), 3707−3717.
(37) De Vos, Y.; Jacobs, M.; Van Der Voort, P.; Van Driessche, I.; Snijkers, F.; Verberckmoes, A. Optimization of Spray Dried Attrition-Resistant Iron Based Oxygen Carriers for Chemical Looping Reforming. *Chem. Eng. J.* **2017**, *309*, 824−839.
(38) Jing, D.; Snijkers, F.; Hallberg, P.; Leion, H.; Mattisson, T.; Lyngfelt, A. Effect of Production Parameters on the Spray-Dried Calcium Manganite Oxygen Carriers for Chemical-Looping Combustion. *Energy Fuels* **2016**, *30* (4), 3257−3268.
(39) Matzen, M.; Pinkerton, J.; Wang, X.; Demirel, Y. Use of Natural Ores as Oxygen Carriers in Chemical Looping Combustion: A Review. *Int. J. Greenhouse Gas Control* **2017**, *65*, 1−14.
(40) Zhao, H.; Tian, X.; Ma, J.; Su, M.; Wang, B.; Mei, D. Development of Tailor-Made Oxygen Carriers and Reactors for Chemical Looping Processes at Huazhong University of Science & Technology. *Int. J. Greenhouse Gas Control* **2020**, *93*, 102898.
(41) Zhao, H.; Tian, X.; Ma, J.; Chen, X.; Su, M.; Zheng, C.; Wang, Y. Chemical Looping Combustion of Coal in China: Comprehensive Progress, Remaining Challenges, and Potential Opportunities. *Energy Fuels* **2020**, *34* (6), 6696−6734.
(42) Wang, K.; Zhao, H.; Tian, X.; Fang, Y.; Ma, J.; Zheng, C. Chemical-Looping with Oxygen Uncoupling of Different Coals Using Copper Ore as an Oxygen Carrier. *Energy Fuels* **2015**, *29* (10), 6625−6635.
(43) Zhao, H.; Wang, K.; Fang, Y.; Ma, J.; Mei, D.; Zheng, C. Characterization of Natural Copper Ore as Oxygen Carrier in Chemical-Looping with Oxygen Uncoupling of Anthracite. *Int. J. Greenhouse Gas Control* **2014**, *22*, 154−164.
(44) Siriwardane, R.; Tian, H.; Simonyi, T.; Poston, J. Synergetic Effects of Mixed Copper-Iron Oxides Oxygen Carriers in Chemical Looping Combustion. *Fuel* **2013**, *108*, 319−333.
(45) Tian, X.; Zhao, H.; Ma, J. Cement Bonded Fine Hematite and Copper Ore Particles as Oxygen Carrier in Chemical Looping Combustion. *Appl. Energy* **2017**, *204*, 242−253.
(46) Tian, X.; Zhao, H.; Wang, K.; Ma, J.; Zheng, C. Performance of Cement Decorated Copper Ore as Oxygen Carrier in Chemical-Looping with Oxygen Uncoupling. *Int. J. Greenhouse Gas Control* **2015**, *41*, 210−218.
(47) Wang, Y.; Tian, X.; Zhao, H.; Liu, K. The Use of a Low-Cost Oxygen Carrier Prepared from Red Mud and Copper Ore for in Situ Gasification Chemical Looping Combustion of Coal. *Fuel Process. Technol.* **2020**, *205*, 106460.
(48) Adánez-Rubio, I.; Abad, A.; Gayán, P.; De Diego, L. F.; García-Labiano, F.; Adánez, J. Identification of Operational Regions in the Chemical-Looping with Oxygen Uncoupling (CLOU) Process with a Cu-Based Oxygen Carrier. *Fuel* **2012**, *102*, 634−645.
(49) Tian, X.; Su, M.; Zhao, H. Kinetics of Redox Reactions of $CuO@TiO_2-Al_2O_3$ for Chemical Looping Combustion and Chemical Looping with Oxygen Uncoupling. *Combust. Flame* **2020**, *213*, 255−267.
(50) Schwebel, G. L.; Leion, H.; Krumm, W. Comparison of Natural Ilmenites as Oxygen Carriers in Chemical-Looping Combustion and Influence of Water Gas Shift Reaction on Gas Composition. *Chem. Eng. Res. Des.* **2012**, *90* (9), 1351−1360.
(51) Mendiara, T.; García-Labiano, F.; Gayán, P.; Abad, A.; De Diego, L. F.; Adánez, J. Evaluation of the Use of Different Coals in Chemical Looping Combustion Using a Bauxite Waste as Oxygen Carrier. *Fuel* **2013**, *106*, 814−826.

https://dx.doi.org/10.1021/acs.energyfuels.0c01023
Energy Fuels 2020, 34, 8587−8599